

## Measurement of fast-changing low velocities by photonic Doppler velocimetry

Hongwei Song, Xianqian Wu, Chenguang Huang, Yangpeng Wei, and Xi Wang

Citation: *Rev. Sci. Instrum.* **83**, 073301 (2012); doi: 10.1063/1.4731014

View online: <http://dx.doi.org/10.1063/1.4731014>

View Table of Contents: <http://rsi.aip.org/resource/1/RSINAK/v83/i7>

Published by the [American Institute of Physics](#).

---

### Related Articles

Powder diffraction from solids in the terapascal regime

*Rev. Sci. Instrum.* **83**, 113904 (2012)

A sealed capsule system for biological and liquid shock-recovery experiments

*Rev. Sci. Instrum.* **83**, 115113 (2012)

Note: Laser Doppler velocimeter using a dual-longitudinal-mode laser source

*Rev. Sci. Instrum.* **83**, 106103 (2012)

Simultaneous measurement of gravity acceleration and gravity gradient with an atom interferometer

*Appl. Phys. Lett.* **101**, 114106 (2012)

High resolution space quartz-flexure accelerometer based on capacitive sensing and electrostatic control technology

*Rev. Sci. Instrum.* **83**, 095002 (2012)

---

### Additional information on *Rev. Sci. Instrum.*

Journal Homepage: <http://rsi.aip.org>

Journal Information: [http://rsi.aip.org/about/about\\_the\\_journal](http://rsi.aip.org/about/about_the_journal)

Top downloads: [http://rsi.aip.org/features/most\\_downloaded](http://rsi.aip.org/features/most_downloaded)

Information for Authors: <http://rsi.aip.org/authors>

## ADVERTISEMENT



**AIP Advances**

Now Indexed in Thomson Reuters Databases

Explore AIP's open access journal:

- Rapid publication
- Article-level metrics
- Post-publication rating and commenting

## Measurement of fast-changing low velocities by photonic Doppler velocimetry

Hongwei Song,<sup>a)</sup> Xianqian Wu, Chenguang Huang,<sup>b)</sup> Yangpeng Wei, and Xi Wang  
 Key Laboratory for Hydrodynamics and Ocean Engineering, Institute of Mechanics, Chinese Academy of Sciences, Beijing 100190, People's Republic of China

(Received 12 April 2012; accepted 11 June 2012; published online 5 July 2012)

Despite the increasing popularity of photonic Doppler velocimetry (PDV) in shock wave experiments, its capability of capturing low particle velocities while changing rapidly is still questionable. The paper discusses the performance of short time Fourier transform (STFT) and continuous wavelet transform (CWT) in processing fringe signals of fast-changing low velocities measured by PDV. Two typical experiments are carried out to evaluate the performance. In the laser shock peening test, the CWT gives a better interpretation to the free surface velocity history, where the elastic precursor, main plastic wave, and elastic release wave can be clearly identified. The velocities of stress waves, Hugoniot elastic limit, and the amplitude of shock pressure induced by laser can be obtained from the measurement. In the Kolsky-bar based tests, both methods show validity of processing the longitudinal velocity signal of incident bar, whereas CWT improperly interprets the radial velocity of the shocked sample at the beginning period, indicating the sensitiveness of the CWT to the background noise. STFT is relatively robust in extracting waveforms of low signal-to-noise ratio. Data processing method greatly affects the temporal resolution and velocity resolution of a given fringe signal, usually CWT demonstrates a better local temporal resolution and velocity resolution, due to its adaptability to the local frequency, also due to the finer time-frequency product according to the uncertainty principle. © 2012 American Institute of Physics. [<http://dx.doi.org/10.1063/1.4731014>]

### I. INTRODUCTION

As a newly developed instrument, photonic Doppler velocimetry (PDV) becomes a promising replacement in situations where VISAR (Velocity Interferometer System for Any Reflector) diagnostics function poorly.<sup>1–3</sup> That the upper limit velocity to be measured is constrained by the electrical bandwidth of acquisition system is well known, questions on how well this technique works on the velocity of low magnitude while changing rapidly have not been fully answered. Essentially, a displacement interferometer, velocity information is encoded in the frequency domain of measured fringes, rather than individual sampled points. Since a complete fringe will not be yielded until the target moves a distance of  $\lambda_0/2$  (half wavelength of the source laser), lower particle velocity means longer time to complete a fringe, hence, lower temporal resolution. Therefore, local temporal resolution of a PDV measurement is strongly depended on the magnitude of instantaneous velocity being measured. From another point of view, there is a competition between temporal and velocity resolution in PDV analysis.<sup>2</sup> However, to obtain a desirable spectrogram, one needs a better velocity resolution to measure velocities of low magnitude, whereas a better temporal resolution to measure velocities of fast changing. This conflict makes measurement of fast-changing low particle velocities with PDV a challenging task. Here “low velocity” refers to velocities in the magnitude of  $10^0$ – $10^1$  m/s, and “fast-changing” refers to accelerations in the magnitude of

$10^9$  m/s<sup>2</sup> and higher. Fast-changing low particle velocities are commonly found in shock compression experiments, e.g., in a laser-driven test, the flyer may accelerate from several meters per second to several kilometer per second within nanoseconds; when impacting a target, the transition from elastic precursor to plastic wave at the back free surface of the target is particularly pertinent to the situation, where the elastic precursor typically in the order of  $10^1$  m/s is determined by the dynamic yield strength of the target material, the plastic wave in the order of  $10^2$ – $10^3$  m/s is determined by the amplitude of shock pressure, and the acceleration during the transition period is typically above  $10^{10}$  m/s<sup>2</sup>.<sup>4–10</sup>

Some researchers resort to the mathematical advances in signal processing method. To date, the primary method for analyzing PDV data is short-time Fourier transform (STFT), the time-resolved frequency spectrogram; hence, the velocity information can be extracted by selecting appropriate time window.<sup>11</sup> However, STFT has difficulty in resolving unstable signals, for example, the interference fringe measured by PDV for a target moving in low and fast-changing velocities, due to the fixed time window and frequency resolution. Avinadav *et al.*<sup>12</sup> reported that the STFT analysis fails to handle fast-varying low velocities, when the instantaneous frequency of the signal changes at a rate comparable to the frequency itself. The continuous wavelet transform (CWT) has recently emerged as an effective mathematical tool for multiresolution decomposition of signals, and it is inherently suitable for unstable signal analysis that require variable time-frequency localizations.<sup>13</sup> Liu *et al.*<sup>9</sup> reported that, compared to STFT, CWT has the advantages of automatic processing and no manual intervening, by using adaptive time

<sup>a)</sup>Electronic mail: songhw@imech.ac.cn.

<sup>b)</sup>Author to whom correspondence should be addressed. Electronic mail: huangcg@imech.ac.cn.

windows to analyze the local frequency of PDV fringe signals. However, one should note that there are an infinite number of wavelet bases or prototype mother wavelets, some may produce drastically different results.<sup>11</sup> In addition, the practical procedure for finding the maximum power of spectrogram, or ridge extraction, subjects many restrictions. Therefore, further discussion about the performance of STFT and CWT is demanded. It should be noted that the quadrature demodulation technique (QDT) is also state-of-the-art unsteady frequency analysis. To overcome the drawback of limited temporal resolution of low frequency signals, Czarske<sup>14</sup> proposed QDT, which allows precise frequency measurements of a pair of signals in quadrature, independently of the number of signal periods or “peaks” available.

We developed a PDV system that basically follows the configuration reported by Strand *et al.*<sup>1</sup> Data processing programs based on STFT and CWT are developed in the MATLAB environment, and practical procedures for mother wavelet selection and ridge extraction are outlined. Particle velocity measurements in laser shock peening (LSP) test and Kolsky-bar based tests with PDV are designed to demonstrate the feasibility of the PDV diagnostic and the performance of STFT and CWT in handling fast-changing low velocities. In the laser shock peening test, the back free surface velocity accelerates from several meters per second to hundreds meters per second within a nanosecond-level short time, after that, the velocity fluctuates significantly due to the propagation of shock waves between the free surfaces. The velocity history is quite different from that of a laser-driven flyer. VISAR (Refs. 4, 5, and 15) and Fabry-Perot interferometer<sup>16</sup> have been used to measured the particle velocity of LSP, however in some VISAR measurements, the elastic precursor has not been tracked. In the Kolsky-bar based tests, the longitudinal velocity of the incident bar and the radial velocity of the shocked sample are detected by PDV. The radial velocity of the sample is typically in sub-meter to two meters per second. It should be noted, that up to now no published experimental data available for radial velocity of the sample measured by PDV. In the recent work by Avinadav *et al.*,<sup>12</sup> a new experimental approach of the Kolsky-bar system with the aid of PDV is reported, the optical measurement of radial expansion rate on the sample itself is optional, but no related result is presented.

Section II gives a brief overview of the PDV principle and theories about the STFT and CWT and their time-frequency resolution, and practical procedures adopted in our data processing program are outlined. Section III describes two types of shock experiments in which particle velocities are measured by PDV, and the detailed comparison of STFT and CWT in each test is carried out based on theoretical explanations.

## II. PRINCIPLES AND METHODS

### A. PDV function

The PDV employs a heterodyne technique, and the heterodyne beat signal is obtained by mixing a reference single frequency laser of  $f_0$  and its Doppler shifted reflection of  $f_b(t)$

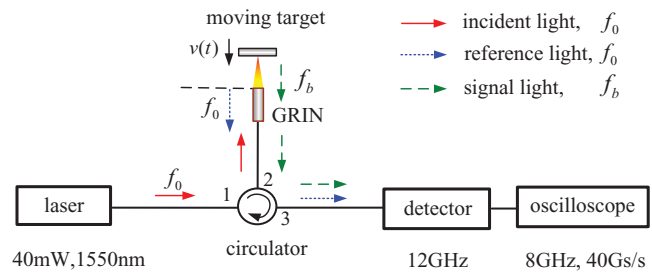


FIG. 1. Configuration of PDV diagnostic.

off a moving target surface. Beat frequency  $\Delta f_b(t) = f_b(t) - f_0$  relates the instantaneous surface velocity by<sup>1</sup>

$$u(t) = \frac{\lambda_0}{2} \Delta f_b(t), \quad (1)$$

where  $\lambda_0$  is the wavelength of source laser. Although there are some recent developments,<sup>17–20</sup> the PDV configuration firstly reported by Strand *et al.*<sup>1</sup> is still very attractive. Our PDV system is depicted in Fig. 1. The source laser is a 1550 nm DFB laser from JDS Uniphase Corporation, the output power is 40 mW, and the linewidth is 200 kHz. Heterodyne beat frequency is detected by using 12 GHz bandwidth InGaAs  $p-i-n$  photodiode detectors from New Focus, Inc., and is recorded by using an 8 GHz digital oscilloscope from Lecoy, Inc. The high speed oscilloscope can record four channels of data at a maximum sampling rate of 40 Gs/s on each channel.

### B. STFT and CWT

The fleeting beats signal needs to be mathematically transformed to the frequency domain for computation of the velocity spectrogram. STFT is a commonly used method in time-frequency analysis, and

$$STFT(\tau, f) = \int x(t)g(t - \tau) \exp(-i2\pi ft) dt, \quad (2)$$

where  $x(t)$  is the signal to be transformed,  $g(t - \tau)$  is the window function with the midpoint position by  $\tau$ . The transformation can be thought of as an expansion in terms of basis functions, which are generated by modulation, and by translation of the window  $g(t)$ , where  $f$  and  $\tau$  are the modulation and translation parameters, respectively. Usually the Hamming window is adopted, and the frequency resolution  $\Delta f$  (therefore, velocity resolution) and the temporal resolution  $\Delta t$  subject to Heisenberg’s uncertainty principle

$$\Delta f \Delta t \geq 1. \quad (3)$$

In the CWT, the signal  $x(t) \in L^2(\mathbf{R})$  is hierarchically decomposed in terms of a family of wavelets which are obtained from a prototype mother wavelet  $\psi(t)$  by dilations and translations<sup>21</sup>

$$W_\psi(a, b) = \frac{1}{\sqrt{|a|}} \int_{-\infty}^{+\infty} x(t) \psi * \left( \frac{t-b}{a} \right) dt, \quad (4)$$

where the asterisk represents operation of complex conjugate, and the scale factor  $a$  and time shift  $b$  are used to operate dilations and translations, respectively. A path that follows the maximum modulus of the CWT  $\max |W_\psi(a, b)|$  is

termed a wavelet ridge, and values of  $a(b)$  along this path give the instantaneous fringe frequency.<sup>22,23</sup> The most commonly used wavelet is the Morlet wavelet, it meets the uncertainty principle

$$\Delta f \Delta t \geq 1/(4\pi). \quad (5)$$

Comparing Eq. (5) with Eq. (3), one finds that the CWT has a better temporal resolution and frequency resolution than STFT, in addition to the advantage of variable time-frequency localizations. Equations (3) and (5) also indicate the competition between temporal resolution and velocity resolution.

### C. Practical procedure

The following procedure is adopted in our CWT program:

- (1) Since there are numerous prototype wavelets, appropriate ones must be selected according to the characteristics of the fringe signal. First, the signal is analyzed by STFT, and the spectrum distribution and velocity range are obtained. Then the mother wavelet is selected according to the calculated power spectrum and bandwidth of STFT.
- (2) Since the CWT is sensitive to the background noise, a frequency bandpass filter is used to eliminate low frequency changes to the signal and high frequency noise, by setting up the lower limit and upper limit velocities according to the STFT spectrogram.
- (3) However, the filter may neglect low velocities at the initial stage of the fringe signal. So, we process CWT with both the filtered signal and the raw signal, then we multiply modulus of wavelet coefficients of the filtered signal  $|W_\psi(a_i, b_i)|_{\text{filter}}$  and those of the original signal  $|W_\psi(a_i, b_i)|_{\text{raw}}$ . Local ridge is obtained by finding the local maximum value of modulus product in the  $(a_i, b_i)$  space.
- (4) Also due to the sensitivity to the background noise, the unstable intensity in signal may cause a breakpoint during ridge extraction. Therefore, we find the location of the maximum value of modulus product throughout the power spectrum as the beginning position for a ridge extraction.

## III. EXPERIMENTAL

### A. Particle velocimetry of laser shock peening

Experimental setup for particle velocimetry of laser shock peening is illustrated in Fig. 2. The 4-mm-thick K9 glass (confined overlay), 0.1-mm-thick Al foil (absorption layer), and 1-mm-thick 2024 Al (target) are fully clamped within a specially designed fixture. A Q-switched high power Nd:YAG laser of 2.5 J per shot with FWHM of 7–10 ns is utilized in the LSP. Upon irradiation, high density plasma is generated from the laser-irradiated absorption layer, and the hydrodynamic expansion of the heated plasma in the confined region between the metal target and the transparent overlay creates a high amplitude, short duration pressure pulse, inducing shock wave propagation into the target. The comparison of back free surface velocity profiles obtained from nu-

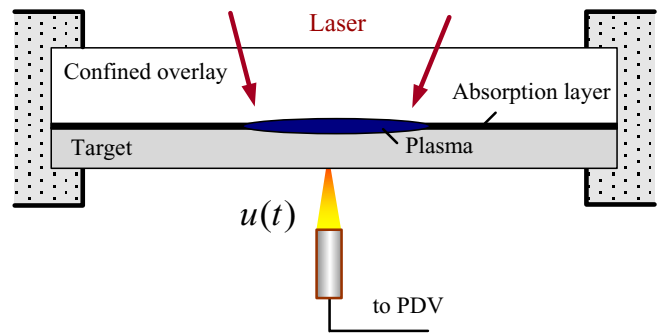


FIG. 2. Particle velocity measurement in laser shock peening.

merical simulation and experimental measurement has been recently reported.<sup>10</sup> Here we give a theoretical prediction, as illustrated in Fig. 3. Since the spatial domain of laser is nearly flat, and the focal diameter (2–3 mm) is effectively larger than the thickness of 2024 Al target (1 mm), it can be approximated to a uniaxial strain condition. When the laser-driven shock pressure is generated, elastic wave begins to propagate. When the shock pressure exceeds  $P_{\text{HEL}}$ , which equals to the Hugoniot elastic limit of the metal target, plastic deformation occurs. The amplitude of plastic wave reaches peak when the shock pressure is the maximum,  $P_{\text{max}}$ . The shock pressure decays well before the arrival of elastic and plastic waves to the back face, and release wave is generated. Therefore, the relationship of shock pressure profile, propagations of elastic wave (1), plastic wave (2), release wave (3), and back free surface velocity history can be predicted, as is shown in Fig. 3.

The CWT spectrogram and STFT spectrogram are shown in Figs. 4(a) and 4(b), respectively, where the extracted ridges or velocity profiles are marked by thin red lines. In Fig. 4(a), structures of elastic precursor wave, main plastic wave, and elastic release wave, which follow the theoretically predicted mechanism, can be clearly identified through the particle velocity profile obtained from CWT method. The lower limit of 16 m/s and upper limit of 400 m/s, corresponding to beat frequencies of 20.6 MHz and 516.1 MHz according to Eq. (1), are selected in the filtering procedure to obtain the present CWT spectrogram. The extracted ridge is 0.2 ns per point, the

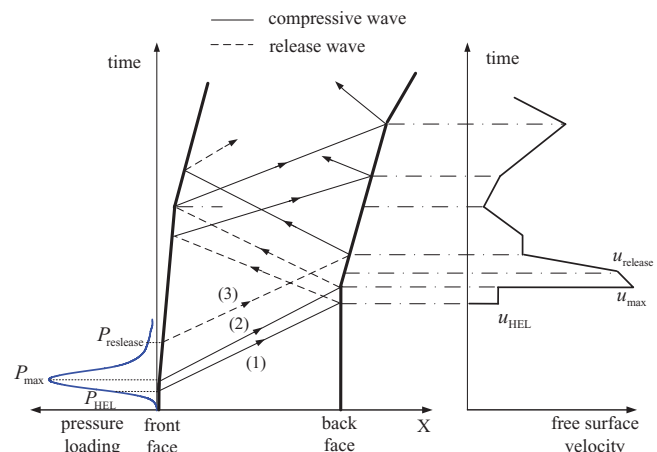


FIG. 3. Shock wave propagation and free surface velocity in the laser shock peening.

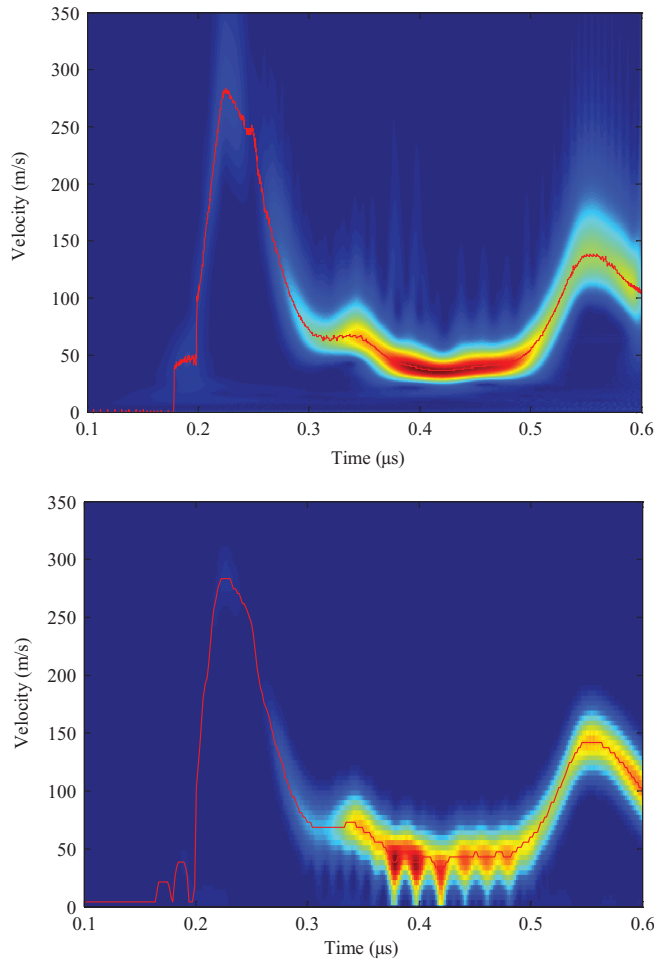


FIG. 4. Comparison of data processing methods for LSP free surface velocity. (a) CWT. (b) STFT.

same as the sampling rate of interference signals. Figure 4(b) shows that STFT fails to interpret the elastic precursor correctly. The STFT spectrogram is obtained by using 22-ns-width Hamming windows and 20 ns overlap between consecutive windows, therefore the exacted ridge is 2 ns per point. According to the uncertainty principle given by Eq. (3), the velocity uncertainty is 35.2 m/s, which is an overly conservative estimation.<sup>2,9</sup> Since the CWT is a multiresolution analysis which scales automatically with local frequency, i.e., uses narrow windows to measure the high frequency components and vice versa, the temporal resolution and velocity resolution of the resolved LSP velocity profile can readily be satisfied. In contrast, the STFT operates with fixed width windows, and this difference determines the time-frequency resolution of each method.<sup>23</sup> An apparent comparison of Figs. 4(a) and 4(b) also indicates that the CWT has denser data points in the ridge, and the spectrogram grain around the ridge is much finer than that of the STFT, indicating better local temporal resolutions and velocity resolutions for the CWT.

More detailed experimental result is shown in Fig. 5, in which the velocity spectrogram is obtained from the CWT. To catch the interference signal at the very beginning, the digital oscilloscope is triggered by the temporal domain of the pulsed laser with a Si biased detector; therefore, the zero point at the

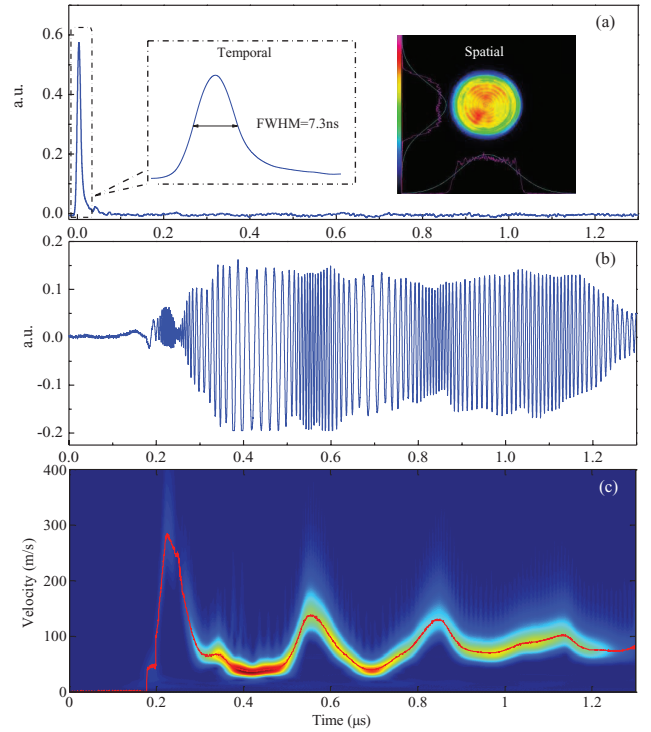


FIG. 5. A typical particle velocity measurement of LSP with PDV (a) temporal and spatial distribution of pulsed laser; (b) fringe signal; (c) velocity history.

horizontal coordinate indicates the onset of laser irradiance. At about 180 ns, the first fringe is observed, indicating the arrival of elastic precursor to the back surface, and the interpreted magnitude is  $u_{\text{HEL}}^{\text{surf}} = 53.4$  m/s. At 224 ns, the free surface velocity reaches the first peak of about  $u_{\text{max}}^{\text{surf}} = 284$  m/s, indicating the first arrival of main plastic shock wave. Therefore, one can estimate that velocities of elastic wave  $C_e$  and plastic wave  $D$  are 6110 m/s and 5140 m/s, respectively, fairly approximate to the documented 6200 m/s and 5520 m/s for 2024 Al.<sup>15</sup>

According to the Rankin-Hugoniot relations for the uniaxial strain state, one can obtain the Hugoniot elastic limit (HEL) for the elastic-plastic target material from the magnitude of elastic precursor<sup>15,24</sup>

$$\text{HEL} = \rho_0 C_e u_{\text{HEL}}^{\text{surf}} / 2. \quad (6)$$

The shock pressure amplitude can be determined from the maximum free surface velocity

$$P_{\text{max}} = \rho_0 \left( C_0 + S \frac{u_{\text{max}}^{\text{surf}}}{2} \right) \frac{u_{\text{max}}^{\text{surf}}}{2} + \frac{2}{3} Y_0 + \Delta P, \quad (7)$$

where  $\rho_0$  is the initial material density,  $C_0$  is the sound velocity at zero pressure,  $S$  is the empirical material parameter,  $Y_0$  is the yield stress, and  $\Delta P$  is the pressure decay when propagates to the back surface. The pressure decay can be determined by the empirical expression from numerical simulations<sup>10</sup>

$$\frac{P}{P_{\text{max}}} = 0.67 \exp\left(-1.41 \frac{H}{2R}\right) + 0.25 \exp\left(-8.33 \frac{H}{2R}\right) + 0.09, \quad (8)$$

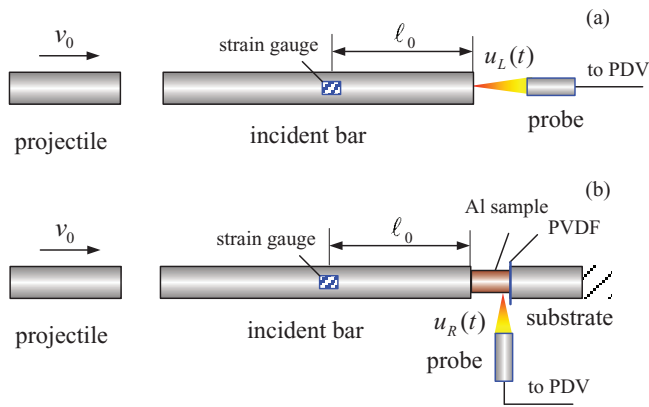


FIG. 6. Velocity measurement of Kolsky-bar based experiments (a) longitudinal velocity of the incident bar; (b) radial velocity of a sample.

where  $H$  and  $R$  are the thickness of target and laser focal radius, respectively. According to Eqs. (6)–(8),  $HEL = 0.459$  GPa for 2024 Al and  $P_{\max} = 3.84$  GPa are obtained from the measured velocity profile.

## B. Particle velocimetry of Kolsky-bar tests

Two types of velocity measurements with PDV are performed on the Kolsky-bar based experiments, one is measuring the longitudinal velocity at the end surface of the incident bar, the other is measuring the radial velocity of the tested sample itself. Experimental setups are depicted in Fig. 6, in each test a strain gauge is attached to the incident bar to provide a triggering signal for data acquisition.

Figure 7 gives the PDV measurement for longitudinal velocity of the incident bar, as well as the strain gauge signal. Dense and distinct fringes are found in the interference signal, and both CWT and STFT interpret the signal well, i.e., the extracted velocity profile is in accordance with the common sense of shock physics. The velocity profile diagnosed by PDV basically follows the shape of the strain gauge signal; however, the rise time of the first peak is a little longer (about  $6.2 \mu\text{s}$  in strain gauge signal and  $11.7 \mu\text{s}$  in velocity profile, respectively), and the oscillations in velocity amplitude after the first peak are more obvious. These phenomena attribute to amplified dispersion effects of transverse inertia as the stress wave propagating along the incident bar.<sup>25</sup> Meanwhile, there are no significant protuberant data in the transformed velocity profiles, indicating the immunity to electronic noise of this non-contact measurement.

In the radial velocity measurement, a cylindrical 2024 Al sample with 10.01 mm in diameter and 9.97 mm in length is placed coaxially between the incident bar and the transmission bar, and the PDV probe is aligned to the radial direction of the sample. Unlike the longitudinal velocity measurement, significant variance in intensity is found in the fringe signal of a radial velocity, and the signal-to-noise ratio (SNR) is low. Figure 8 shows that the CWT improperly interprets the initial part of the signal, while STFT gives a better interpretation.  $4.4 \mu\text{s}$  Hamming windows and  $4 \mu\text{s}$  overlap between the consecutive windows are used in the STFT, corresponding to velocity uncertainty of 0.176 m/s. Results show that STFT is

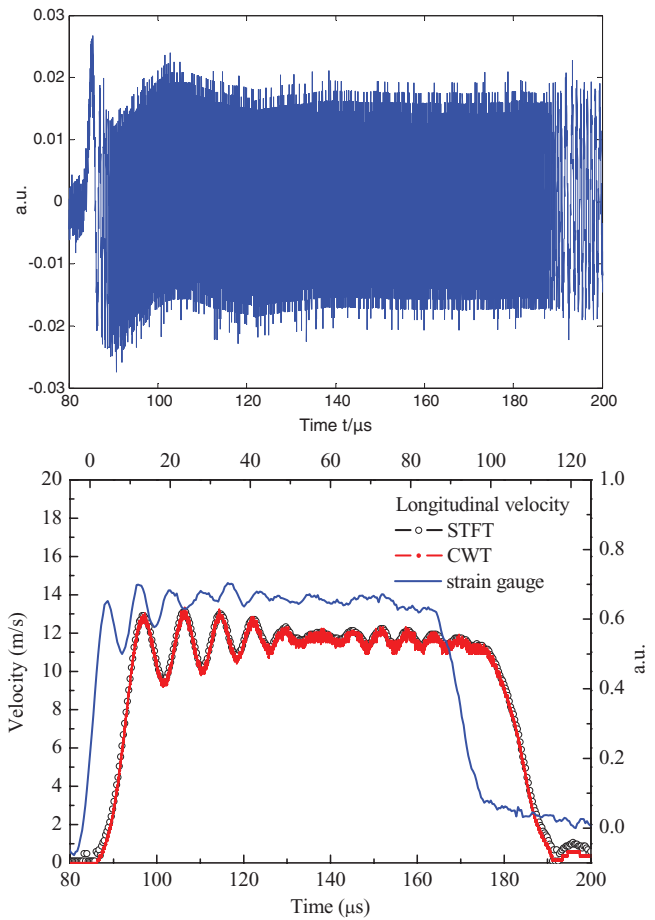


FIG. 7. Longitudinal velocity of incident bar (a) fringe signal; (b) velocity histories obtained from STFT and CWT, and the strain gauge signal.

insensitive to the amplitude and baseline changes, and reliable velocity information can be extracted even at relatively low SNR. The radial velocity of shocked sample is usually at a magnitude of about 2 m/s. Since the PDV probe does not move with the shocked sample, the measured velocity is an Euler velocity rather than a Lagrange velocity.

At the elastic deformation stage, the longitudinal strain  $\varepsilon_l(X, t)$  relates the transverse velocity  $u_R(t)$  by

$$\varepsilon_l(X, t) = -\frac{1}{\nu R} \int_0^{t_c} u_R(t) dt, \quad (9)$$

where  $\nu$  is Poisson's ratio,  $R$  is the original radius of the sample. At the plastic deformation stage, the relation is

$$\varepsilon_l(t) = -\int_{t_c}^t \frac{2u_R(t)}{R(t)} dt. \quad (10)$$

Therefore, the longitudinal strain history can be obtained from the non-contact radial velocity measurement. In a traditional Kolsky-bar test, strains are recorded by strain gauges attached in the bars, rather than a direct measurement of the tested sample itself. Experimental results are greatly affected by the adhesion quality of strain gauges, wave shape dispersion during propagation, and electronic noise, etc. When a polyvinylidene fluoride (PVDF) piezoelectric thin-film sensor is sandwiched between the sample and the substrate, as illustrated in Fig. 6(b), the stress pulse can be recorded.

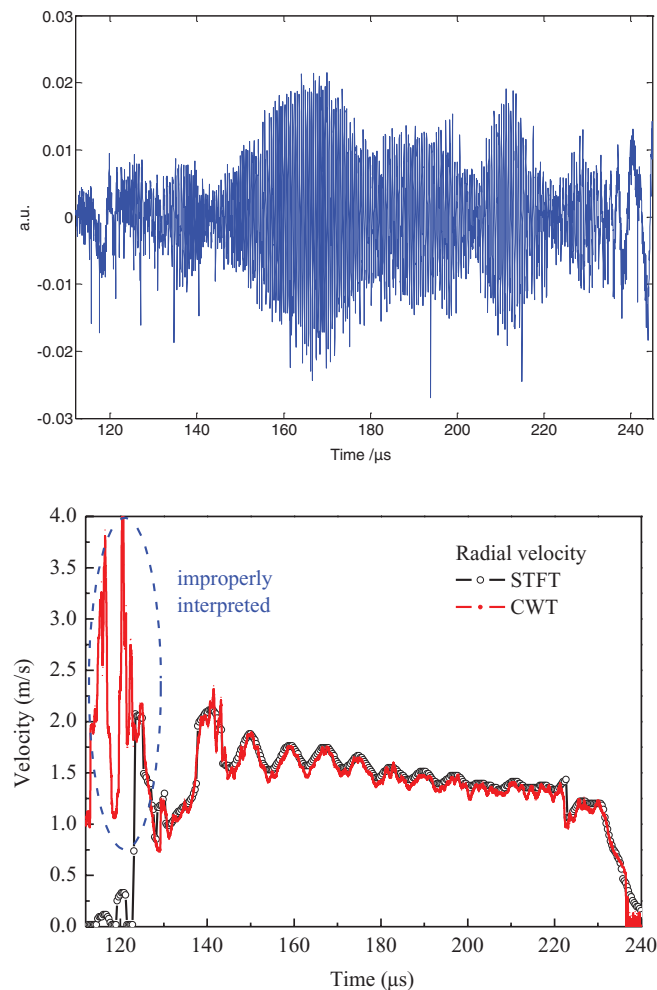


FIG. 8. Radial velocity of a sample (a) fringe signal; (b) velocity histories obtained from STFT and CWT.

Subsequently, the dynamic strain-stress relationship of sampled material can be obtained, by combining longitudinal strain profile deduced from radial velocity of the sample measured by PDV, and longitudinal pressure measured by PVDF. This can be treated as an effective approach that is potentially new for measuring dynamic properties of materials.

#### IV. SUMMARY

The paper makes a further demonstration that PDV diagnostic is capable to capture low particle velocities while changing rapidly. In the measurement of back free surface velocity of LSP, physical phenomena that are perfectly accorded to theoretical analysis are observed. Credible estimations of the velocities of stress waves, Hugoniot elastic limit, and the amplitude of shock pressure induced by laser can be arrived from the PDV measurement. Especially, the PDV captured the elastic precursor during the LSP, with the aid of CWT. Usually VISAR has difficulty in tracking such a low, rapidly changing velocity. In the Kolsky-bar based experiments, the radial velocity of the sample as low as about 1–2 m/s measured by PDV is for the first time reported. Combining the longitudinal stress profile measured by PVDF and the strain profile deduced from radial velocity measured by

PDV, the dynamic strain-stress relationship of sampled material can be obtained, which may be a promising new approach in determining dynamic properties of materials. Experimental results also indicate that, although the intensity of interference signal fluctuates significantly, as shown in Figs. 5(b) and 8(a), the effective velocity history can be extracted, since the velocity information is encoded in the frequency domain. This property makes PDV adaptable to various environments; hence, a popular diagnostic that can be applied in many fields.

Both STFT and CWT have their advantages and disadvantages. The STFT is an efficient transform method, which is robust to low signal-to-noise ratio, but it has difficulty in handling unstable signals, and has poor temporal resolutions and velocity resolutions. It can be used in dealing with signals of poor SNR, such as the radial velocity of the sample in a Kolsky-bar test. In dealing with velocity that is changing extremely fast like a LSP process, STFT is not preferred. CWT demonstrates its adaptability to the unstable signals with flexible analysis time window, and it has better temporal resolutions and velocity resolutions, but it is sensitive to the background noise. Typically the CWT is more favorable in processing fast-changing low velocities.

#### ACKNOWLEDGMENTS

This work is funded by the Instrument Project of Chinese Academy of Sciences (CAS) (Grant No. YZ200930), additional funding is also provided by the National Natural Science Foundation of China (NNSFC) (Grant Nos. 91016025, 10972228, and 11002150). The authors would like to thank Dr. J. Wang and Professor C. Q. Wu at Beijing Jiaotong University for discussion on the data processing method of STFT and CWT.

- <sup>1</sup>O. T. Strand, D. R. Goosman, C. Martinez, T. L. Whitworth, and W. W. Kuhlow, *Rev. Sci. Instrum.* **77**, 083108 (2006).
- <sup>2</sup>D. H. Dolan, *Rev. Sci. Instrum.* **81**, 053905 (2010).
- <sup>3</sup>B. J. Jensen, D. B. Holtkamp, P. A. Rigg, and D. H. Dolan, *J. Appl. Phys.* **101**, 013523 (2007).
- <sup>4</sup>L. Tollier and R. Fabbro, *J. Appl. Phys.* **83**(3), 1231–1237 (1998).
- <sup>5</sup>L. Tollier, R. Fabbro, and E. Bartnicki, *J. Appl. Phys.* **83**(3), 1224–1230 (1998).
- <sup>6</sup>P. Peyre, L. Berthe, R. Fabbro, and A. Sollier, *J. Phys. D* **33**(5), 498–503 (2000).
- <sup>7</sup>J. D. Weng, X. Wang, Y. Ma, H. Tan, L. C. Cai, J. F. Li, and C. L. Liu, *Rev. Sci. Instrum.* **79**, 113101 (2008).
- <sup>8</sup>J. P. Cuq-Lelandais, M. Boustie, L. Berthe, T. de Resseguier, P. Combis, J. P. Colombier, M. Nivard, and A. Claverie, *J. Phys. D* **42**, 065402 (2009).
- <sup>9</sup>S. X. Liu, D. T. Wang, T. Li, G. H. Chen, Z. R. Li, and Q. X. Peng, *Rev. Sci. Instrum.* **82**, 023103 (2011).
- <sup>10</sup>X. Q. Wu, Z. P. Duan, H. W. Song, Y. P. Wei, X. Wang, and C. G. Huang, *J. Appl. Phys.* **110**, 053112 (2011).
- <sup>11</sup>A. R. Valenzuela, G. Rodriguez, S. A. Clarke, and K. A. Thomas, *Rev. Sci. Instrum.* **78**, 013101 (2007).
- <sup>12</sup>C. Avinadav, Y. Ashuach, and R. Kreif, *Rev. Sci. Instrum.* **82**, 073908 (2011).
- <sup>13</sup>A. H. Najmi and J. Sadowsky, *Johns Hopkins APL Tech. Dig.* **18**, 134–140 (1997).
- <sup>14</sup>J. W. Czarske, *Meas. Sci. Technol.* **12**(5), 597–614 (2001).
- <sup>15</sup>L. Berthe, R. Fabbro, P. Peyre, L. Tollier, and E. Bartnicki, *J. Appl. Phys.* **82**(6), 2826–2832 (1997).
- <sup>16</sup>M. Arrigoni, J. P. Monchalain, A. Blouin, S. E. Kruger, and M. Lord, *Meas. Sci. Technol.* **20**, 015302 (2009).

- <sup>17</sup>J. Benier, P. Mercier, E. Dubreuil, J. Veaux, and P. A. Frugier, in *Proceedings of the 9th International Conference on the Mechanical and Physical Behaviour of Materials under Dynamic Loading, Dymat 2009* (E D P Sciences, France, 2009), Vol. 1, pp. 289–294.
- <sup>18</sup>P. Mercier, J. Benier, P. A. Frugier, G. Contencin, J. Veaux, S. Lauriot-Basseuil, and M. Debruyne, *Proc. SPIE* **7126**, 712610 (2008).
- <sup>19</sup>K. G. Krauter, G. F. Jacobson, J. R. Patterson, J. H. Nguyen, and W. P. Ambrose, *Rev. Sci. Instrum.* **82**, 045110 (2011).
- <sup>20</sup>J. D. Weng, X. Wang, T. J. Tao, C. L. Liu, and H. Tan, *Rev. Sci. Instrum.* **82**, 123114 (2011).
- <sup>21</sup>M. Haase and J. Widjajakusuma, *Int. J. Eng. Sci.* **41**(13–14), 1423–1443 (2003).
- <sup>22</sup>L. R. Watkins, *Opt. Lasers Eng.* **45**(2), 298–303 (2007).
- <sup>23</sup>L. R. Watkins, *Opt. Lasers Eng.* **50**(8), 1015–1022 (2012).
- <sup>24</sup>R. Fabbro, P. Peyre, L. Berthe, and X. Scherpereel, *J. Laser Appl.* **10**(6), 265–279 (1998).
- <sup>25</sup>M. A. Meyers, *Dynamic Behavior of Materials* (Wiley, 1994).